3D Printed Polypropylene-Based Multifunctional Skin-Core Structures for Thermal Conductivity

Polymer Composites

WILEY | spe INSPIRING PLASTICS PROFESSIONALS

RESEARCH ARTICLE OPEN ACCESS

3D Printed Polypropylene-Based Multifunctional Skin-Core Structures for Thermal Conductivity

Eleonora Lorenzi[1,2] | Rossella Arrigo[1,2] | Alberto Frache[1,2]

[1]Department of Applied Science and Technology, Polytechnic of Turin, Alessandria, Italy | [2]Local INSTM Unit, Alessandria, Italy

Correspondence: Alberto Frache (alberto.frache@polito.it)

Received: 6 March 2025 | **Revised:** 29 April 2025 | **Accepted:** 16 May 2025

Keywords: fused filament fabrication (FFF) | mechanical properties | multi-material additive-manufacturing | polypropylene | talc

ABSTRACT

In this work, polypropylene (PP)-based filaments for Fused Filament Fabrication (FFF) containing boron nitride (BN) and talc (T) were developed, aiming at formulating multi-material 3D printed parts showing thermal conductivity and balanced mechanical properties. Particularly, skin-core structures obtained by localizing BN in the surface layers while confining T in the core were 3D printed and characterized, and their properties were compared to those of correspondent mono-material samples. The characterization of the PP/BN mono-material samples revealed a crucial role of the FFF process in inducing higher thermal conductivity in the radial direction of the specimens as compared to the axial one, owing to the preferential alignment of the fillers along the printing direction allowing the creation of continuous conductive paths in the in-plane direction. For the multi-material structures, it was demonstrated that confining the thermally conductive fillers to the surface of the samples allows achieving higher in-plane thermal conductivity as compared to PP/BN samples; for instance, nearly doubled values were obtained by decreasing the number of BN-containing layers from 15 to 3. Most importantly, the skin-core structures exhibit tensile modulus and stress practically identical to those of PP/T mono-material samples, despite the lower content of the reinforcing filler and the presence of interfaces between the two different composites.

1 | Introduction

The Fused Filament Fabrication (FFF) process offers several advantages over traditional manufacturing, including the ability to produce components with highly intricate geometries and internal voids, easy customization without the need for new molds, and reduced material waste, making it more sustainable and cost-effective [1–3]. Additionally, the ability to use multiple materials in a single print offers endless possibilities for creating innovative skin-core multi-material components [4–6]. By using composite polymers with specific properties, achieved through the addition of reinforcing and functional fillers, the ability to precisely localize these materials in specific areas of the object unlocks the potential to create multifunctional components with varied and tailored properties that would otherwise be difficult to achieve with more traditional manufacturing techniques, such as press stacking or co-injection molding [7–9]. In fact, 3D printing is a continuous process that, in a single production step, allows for high precision and control over the thickness of the skin layer, along with complete freedom in choosing the exact localization of the functionalized material, with the ability to follow specific designs and geometries according to the requirements. For instance, Regazzi et al. [10] developed through additive manufacturing flame-retarded polylactic acid-based skin/core structures, by localizing the flame retardant system only at the surface of the material exposed to the flame or radiant heat. It was demonstrated that selectively concentrating the flame retardant on the sample surface dramatically improved the fire behavior, whereas the same amount of flame retardant distributed throughout the sample was inefficient.

From a general point of view, multi-material 3D printing processes offer the possibility to keep the core of the component filler-free or strengthen it with a reinforcing filler, while localizing the functional fillers only where the functionality is most required; this strategy allows obtaining components that simultaneously exhibit the desired characteristics on the surface and good mechanical properties. Nevertheless, the achievement of mechanical properties equivalent to those of parts manufactured through traditional processing technologies (such as injection or compression molding) is still a challenging issue in the 3D printing of multi-material structures [11]. The main reason is related to the typically weak interface bonding between the different materials, which dramatically affects the mechanical properties of the 3D printed part [12]. In fact, by using immiscible materials, as well as the same polymer but containing different types of fillers, the intermolecular diffusion between subsequently deposited layers is limited, resulting in physical discontinuities at the interface that cause a worsening of the mechanical properties [13].

The transition of 3D printing from a technique primarily used for rapid prototyping to a process for the production of highly customizable and functional parts for high-end engineering applications depends largely on the selection of materials. For this reason, in this study, polypropylene (PP) was chosen as the polymer matrix instead of polylactic acid or other more commonly used materials in FFF processes. Despite the fact that the use of PP in additive manufacturing is still rare due to the various challenges it presents during the 3D printing process (such as shrinkage and detachment from the print bed), several studies have shown that its printability can be improved by using copolymers [14, 15] or polymer blends [16], and through the addition of fillers such as carbon fibers [17], talc [18, 19], rubber crumbs [20], husk particles [21], and nanoclay [22, 23].

In this work, filaments based on a heterophasic PP copolymer and two types of fillers (namely, hexagonal boron nitride (h-BN) and talc (T)) were formulated and printed through FFF, aiming at creating 3D printed skin-core structures that exhibit both improved surface thermal conductivity and good mechanical properties. In fact, h-BN possesses a honeycomb atomic structure similar to that of graphene and a lamellar morphology, but shows distinct properties; in fact, due to the absence of free-moving electrons, the thermal conductivity is completely determined by phonons. This property allows boron nitride to be an excellent electrical insulator (electrical resistivity: $3 \times 10^7\,\Omega\,cm$), while simultaneously exhibiting high thermal conductivity (in-plane of 600 W/mK and through-plane of 30 W/mK) [24]. Conversely, talc has been employed as a reinforcing filler to enhance the mechanical properties of the polymer matrix [25].

The work can be divided into three parts. The first part focused on the production of PP-based filaments suitable for 3D printing, filled with BN or talc, and on the evaluation of their printability.

In the second part, the effect of the 3D printing process on thermal conductivity values, in the in-plane and through-plane directions of the samples, was evaluated through thermal conductivity measurements on 3D printed specimens. Finally, in the third part, multi-material combined and skin-core 3D structures, based on the PP/BN and PP/talc composites, were studied.

2 | Materials and Methods

2.1 | Materials

Polypropylene (PP) ISPLEN PB 170 G2M from Repsol Chemicals (Madrid, Spain) was used. This is a polypropylene-polyethylene random copolymer (density of 905 kg/m^3 and melt flow index of 12 g/10 min (230°C, 2.16 kg)).

As fillers, boron nitride from Sigma-Aldrich (average particle size: ~1 μm) (Darmstadt, Germany) and talc HTP1 grade (mean diameter of 1.9 μm, density of 2.8 g/cm^3), supplied by IMI Fabi Spa (Valmalenco, Italy), were used.

2.2 | Preparation of the Composites

The four PP-based composites, containing respectively 15 wt% BN (15BN), 20 wt% BN (20BN), 30 wt% BN (30BN) and 30 wt% talc (30T), were prepared through melt compounding using a co-rotating twin-screw extruder LEISTRITZ ZSE 18/40 D. The heating temperature was set at 190°C in all eight thermostated barrel blocks, and the screw rotation speed was set at 200 rpm. Two gravimetric feeders were used: the main hopper for the polymer and the side feeder for the filler.

A hot plate press Collin P 200T (Maitenbeth, Germany) was used to obtain the samples for the rheological tests (25 mm diameter for 1 mm thickness). The operation was carried out by pressing the pellets at 100 bar into a right-shaped metallic mold for 2 min. The temperature used was 190°C for the pristine PP and 220°C for the compounds.

2.3 | Filament Formulation

Compatible filaments for the 3D printer, with a diameter of 1.75 mm, were produced with a Felfil Evo filament making machine (Torino, Italy), which is composed of a single-screw extruder, a mobile cooling fan array, and a spooler with two rollers, a diameter sensor, and a spool holder. Processing parameters such as extrusion temperature, screw speed, power, and position of the fans can be optimized depending on the material used, while the speed of the rollers is automatic and automatically self-adjusts in order to maintain the set diameter value.

The optimization of parameters for each formulation was carried out by adjusting three main factors: extrusion temperature, screw speed, and the distance of the fan array from the extruder (Table 1). Other settings were kept unchanged for all filaments: filament diameter of 1.75 mm, spooler speed at 75 rpm, and fan speed at 180 (with the maximum fan speed being 255).

The optimization of the process began with the selection of the extrusion temperature and screw speed, as these parameters are essential to ensure a steady and consistent flow of material from the extruder.

Furthermore, concerning the position and speed of the cooling fans, it was observed that a fan power of 180 (70% of the maximum power) was suitable for all the different formulations, as

lower or higher values led to inconsistent diameters and cross-sections of the filaments. The position of the fans relative to the extruder head was varied; however, generally, distances greater than 4 cm caused the extruded filament to bend under the action of gravity before it could reach the cooling system.

2.4 | Three-Dimensional Printing Equipment

The 3D printer FlashForge Creator 3 Pro (Zhejiang, China), equipped with a 0.4 mm steel nozzle, was used to 3D print two different types of specimens: disks with a diameter of 25 mm and a thickness of 3 mm for thermal conductivity measurements, and tensile test specimens (ISO-527A-5A) for mechanical tensile testing. In both cases, monomaterial specimens and skin-core structures were created by combining the 30BN and 30T composites, varying the number of layers made with each material (the total number of layers for all samples is 15). Figure 1 presents a diagram of all the specimens studied along with their respective nomenclature. It is important to note that for the monomaterial specimens, the name refers to the material used, while for the skin-core structures, the number indicates the number of layers containing BN or talc (e.g., the 3BN + 12T consists of 3 layers filled with 30 wt% BN and 12 layers filled with 30 wt% talc).

Since PP shows very poor adhesion on any material different from PP itself, a polypropylene 3D printing bed and a 3D-printing adhesive for PP (Magigoo, Curmi, Malta) were used. The optimized parameters used for the different composites will be discussed in Section 3.4.

2.5 | Characterization Techniques

2.5.1 | Thermal Properties

The thermal properties of the produced materials were assessed using Differential Scanning Calorimetry (DSC) with a DSC Q20 by TA Instruments (New Castle, DE, USA). Samples were placed in a nitrogen-controlled chamber and heated from 50°C to 250°C at a rate of 10°C/min, then cooled back to 0°C at the same rate, followed by reheating to 250°C with a 10°C/min ramp. The results obtained from this analysis are: Crystallization temperature (T_c), Melting temperature (T_m) and Melting Enthalpy (ΔH_m), evaluated as the area under the endothermal peak of the heat flow during the second heating cycle. To calculate the crystallinity percentage (X_c) of the PP-based compounds, the following formula (Equation 1) has been used:

$$X_c = \frac{\Delta H_m}{(1-x)\,\Delta H_m^0} \quad (1)$$

where ΔH_m is the melt crystallization enthalpy, $\Delta H_m{}^0$ represents the melting enthalpy of the 100% crystalline PP, and x is the filler weight fraction. The value of 207 J/g has been considered as a reference for the 100% crystalline PP melting enthalpy.

TABLE 1 | Optimized parameters for filaments' extrusion process.

Material	T_{extr} [°C]	Screw speed [rpm]	Fan distance [cm]
PP	190	3	2
30T	200	3	2
15BN	190	3	4
20BN	190	2	0
30BN	200	4	4

2.5.2 | Rheological Analysis

To evaluate the rheological properties of the unfilled PP and PP-based composites, an ARES (TA Instrument, USA) strain-controlled rheometer in parallel plate geometry (plate diameter = 25 mm) was used. For each sample, preliminary strain sweep tests were carried out at 260°C and a frequency of 10 rad/s in order to select a strain amplitude in the linear viscoelastic region. Then, the complex viscosity, storage, and loss moduli were measured by performing frequency sweep tests from 100 to 0.1 rad/s.

2.5.3 | Morphology

Both the section of the filaments and of the 3D printed specimens were investigated using an EVO 15 Scanning Electron Microscope (SEM) from Zeiss (beam voltage: 20 kV; working distance: 8.5 mm, Oberkochen, Germany). The investigated surfaces were prepared by fracturing the samples in liquid nitrogen and then covering them with a sputtered gold layer. Quantitative compositional information was achieved using Energy Dispersive x-ray Spectroscopy (EDX). To evaluate the amount and dimension of voids present in the 3D-printed samples and their general quality, x-ray computed tomography images were obtained using the CT-ALPHA system with a MicroFocus 240 kV x-Ray Source by ProCon x-Ray GmbH (Sarstedt, Germany) and the data elaboration was done with myVGL software (Volume Graphics GmbH).

2.5.4 | Tensile Characterization

An Instron 5966 (Norwood, MA, USA) equipped with a 2 kN load cell was used to perform the tensile tests. A crosshead speed

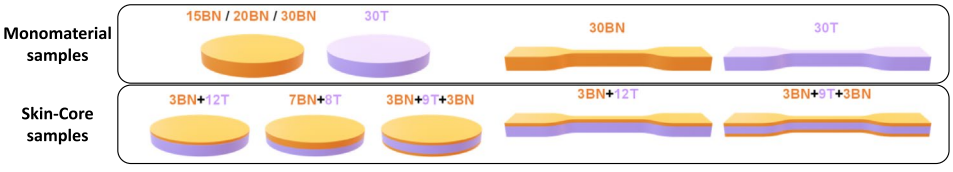

FIGURE 1 | Diagram of all the 3D printed monomaterial and skin-core sample.

of 1 mm/min was applied and maintained up to the achievement of 0.25% deformation and was then increased up to 10 mm/min until breaking. The tests were carried out on five specimens, and the results were averaged.

2.5.5 | Thermal Conductivity

Due to the strong anisotropy of the 3D printed specimens, the thermal conductivity in the in-plane (IP) and through-plane (TP) directions was evaluated with an anisotropic method using the transient plane heat source method (ISO 22007-2:2022) with a TPS 2500S by Hot Disk (Göteborg, Sweden). All tests were carried out with a 5465 Kapton sensor (radius 3189 mm) and with a value of heat power of 10 mW. The measuring setup was inserted in a container dipped in a silicon oil bath (Haake A40, Thermo Scientific Inc., Waltham, MA, USA) equipped with a temperature controller (Haake AC200, Thermo Scientific Inc., Waltham, MA, USA) in order to control the temperature at 23.00°C ± 0.01°C.

3 | Results

3.1 | Rheological Characterization

As with all plastic processing and transformation methods, it is crucial to assess the rheological behavior of materials in the 3D printing process, in order to determine their processability and, consequently, their suitability for 3D printing [26]. The complex viscosity of the polymer matrix and all composites was studied through dynamic frequency sweep tests. The complex viscosity curves as a function of frequency are shown in Figure 2.

Unfilled PP is characterized by a Newtonian plateau at low and intermediate frequencies, with a slight decrease in viscosity at higher frequencies (mild shear thinning behavior), clearly indicating that the polymer matrix exhibits a pronounced Newtonian behavior.

By observing the trends of complex viscosity related to the composites, it is evident that the addition of both fillers generally leads to an amplification of the non-Newtonian behavior of the material. The embedded solid fillers, through their interaction with the macromolecules, restrict the movement of polymer chains, thereby hindering their complete relaxation. As a consequence, an increase in viscosity occurs at low frequency values, indicating the appearance of yield stress. Regarding composites containing BN, it is observed that as the filler percentage increases, yield stress progressively rises. This indicates that higher filler quantities facilitate the creation of more filler-filler and filler-polymer interactions, leading to a more interconnected and rigid network within the material, which becomes increasingly effective in limiting the mobility of macromolecules [27]. Along with the increase in yield stress, a more pronounced shear thinning effect at higher frequency values can also be observed, which is milder in the case of 15BN and significantly more marked in the cases of 20BN and 30BN. Considering now the 30T composite, it can be observed that it exhibits a viscosity increase at low frequencies similar to the 30BN composite, but

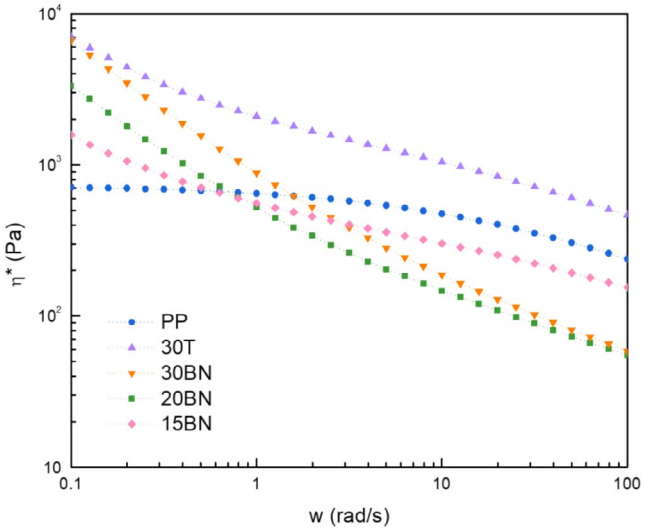

FIGURE 2 | Complex viscosity curves of PP and PP-based composites (the dotted lines are just an eye-guide).

with less pronounced shear thinning. This difference can be attributed to the varying average sizes and aspect ratios of the two fillers. In particular, talc particles have larger dimensions and a lower aspect ratio compared to BN platelets. This means that, under conditions of equal weight percentage, the polymer/filler interface is smaller in the case of talc, resulting in fewer interactions and, consequently, less interference with the relaxation dynamics of the PP macromolecules.

Considering the processability of these materials, a pronounced non-Newtonian behavior is advantageous for the FFF process, as it ensures appropriate viscosity throughout printing. Low viscosity under high shear rates when passing through the nozzle ensures good melt flow and prevents clogging [28–30]. Conversely, a rapid viscosity increase at lower shear rates, at the nozzle exit, helps retain the extrudate shape throughout the stand-off region and on the printing platform. Adequate viscosity is also necessary to ensure good interlayer adhesion, which is essential for achieving strong and stable printed structures [31]. It is therefore evident that all the composites exhibit superior FFF-printability compared to pristine PP. However, for the production of the skin-core structures, only the two composites with the most pronounced non-Newtonian behavior, 30BN and 30T, were used.

3.2 | Thermal Characterization

DSC analyses were performed on the unfilled matrix and all the formulated compositesto evaluate the content of crystallinity, which is directly correlated to the volumetric shrinkage of the material [32–34].

From the results in Table 2 (the recorded thermograms are reported in Figure S1), it can be observed that the addition of fillers does not significantly alter the crystallinity of the PP macromolecules. However, it is evident that the addition of fillers leads to a decrease in melting enthalpy (ΔH_m), and consequently, to a reduction of the crystalline phase fraction in the printed parts, which corresponds to reduced volumetric

shrinkage. Specifically, the addition of 30 wt% of both talc and boron nitride results in the lowest melting enthalpy values. This indicates that the 30T and 30BN materials not only exhibit better 3D printability in terms of rheological behavior (as observed in Section 3.1), but also improved dimensional stability. Similar results regarding the reduction of melting enthalpy in PP-based composites for FFF, filled with h-BN, were obtained by Li et al. [35].

3.3 | Filament Production Optimization

In order to evaluate the quality of the filaments produced through the optimization discussed in Section 2.3, SEM analyses were conducted, focusing on both the cross-section and the outer surface. Figure 3a,c, illustrate the cross-sections of the 30BN and 30T filaments, respectively, showing that the filaments exhibit an almost perfectly circular cross-section. Figure 3b,d, present the outer surfaces, which appear to be smooth and free of significant defects. Additionally, the measured diameters of the filaments remain almost constant and within the range of 1.75 ± 0.1 mm. Based on these observations, it is possible to conclude that the filaments possessed suitable characteristics for the FFF process [36].

TABLE 2 | Scanning calorimetry data of the materials.

Material	T_m [°C]	T_c [°C]	ΔH_m [J/g]	χ_c [%]
PP	164	110	82	40
30T	166	126	61	42
15BN	165	121	80	45
20BN	164	122	71	43
30BN	164	122	60	41

3.4 | Three-Dimensional Printing

An optimization of the printing parameters was conducted for all specimens to minimize the presence of voids, porosity, and warpage. A layer thickness of 0.2 mm, a 100% infill, and an infill pattern of ±45° were used for all specimens. Regarding the temperatures, while the extrusion temperature was maintained constant at 260°C for all composites, the printing bed temperature was adjusted to optimize the adhesion of the printed object to the platform and thus reduce warpage. In general, the talc-reinforced composite was easier to 3D print compared to the one with BN. For the PP with talc, a printing bed temperature of 50°C was sufficient, whereas for the specimens of PP and PP filled with BN, it was necessary to raise the temperature to 70°C and additionally employ a 3D-printing adhesive for PP.

In the specific case of the tensile test specimens, due to their elongated shape, the effect of warpage was more pronounced. In particular, for the monomaterial specimen 30BN, it was necessary to use a raft, which was constructed using the composite 30T. This approach took advantage of the excellent adhesion properties of this material to both the printing platform and the composite containing BN. In fact, even in the printing of the skin-core structures, the combination of the two different materials did not present any issues. On the contrary, the presence of 30T layers at the bottom of the specimens appeared to facilitate the deposition of 30BN. This aspect will be further explored in the following sections.

3.5 | SEM and Tomography

To assess the quality of the printed specimens in terms of the presence of voids and adhesion between the layers, SEM analyses and tomography were performed. These tests were particularly

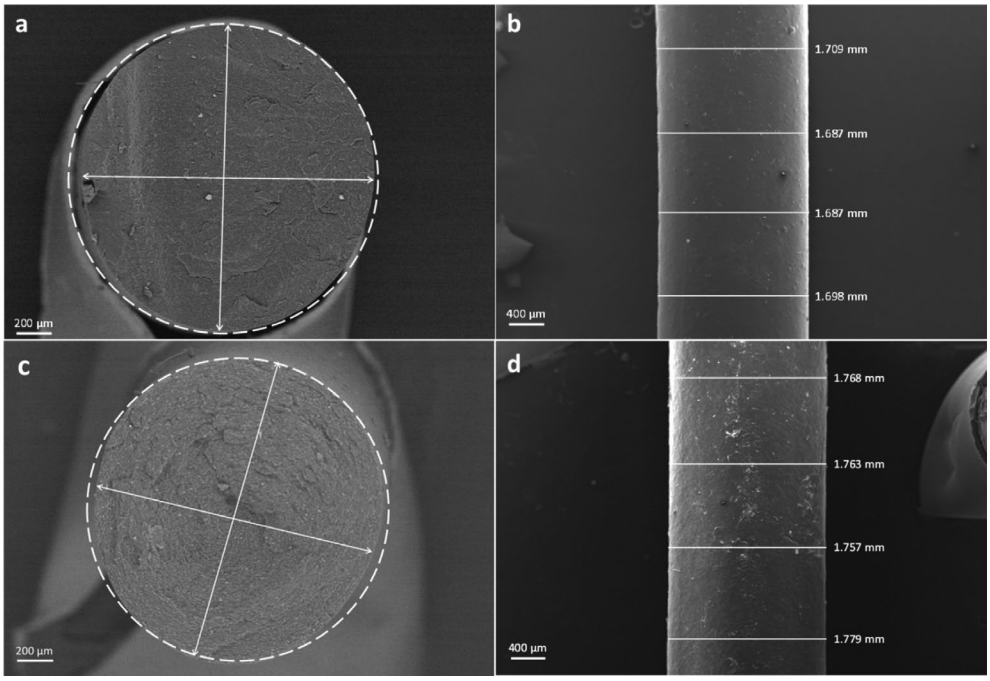

FIGURE 3 | SEM micrographs of the filament's cross-section (100×) and surface (50×): (a, b) 30BN, (c, d) 30T.

crucial for evaluating the compatibility between the two different composites used in the formulation of the skin-core structures. In fact, to ensure both good mechanical properties and thermal conductivity, it is essential to achieve a strong interlayer bond through molecular interdiffusion and entanglement across the inter-filament interfaces [12, 31].

Figure 4a presents a representative SEM micrograph of the specimen 3BN + 9T + 3BN, in which the distinct layers containing the different fillers are clearly visible. Figure 4b shows an enlarged view of the interface between the 30BN and 30T layers, demonstrating perfect adhesion between them. Confirmation that we are indeed at the interface between the two composites is provided by the elemental mapping of silicon, magnesium, and nitrogen from the EDX analysis, which clearly shows that the elements constituting talc, such as Si and Mg (Figure 4c,d), are localized in the upper region, while N (Figure 4e), present in boron nitride, is located in the lower region.

From the SEM images of the cross-section of the specimens, it is also possible to observe the orientation of the fillers inside the filament. Keeping in mind that all samples were printed with a raster angle of ±45° (as illustrated in Figure 5a), in the SEM micrograph in Figure 5b, the y–z cross-section of the layers filled with talc of the 3BN + 12T specimen is visible. The clear alternation between the filaments deposited in the x and y directions can be observed, as well as how the filler lamellae preferentially align in the printing direction. A similar orientation of the filler, due to a deposition-induced effect, was observed by Luo et al. [37] in 3D printed TPU/BN composites and by Jia et al. [38] in the case of graphite flakes in a PA6/POE-g-MAH/PS matrix. From the enlargement in Figure 5c, the sections of the deposited filaments along the x-axis can be identified. Within these filaments, talc lamellae are observed to be aligned along the same direction and concentric to the filament.

As already widely documented in the literature, the alignment of embedded particles along the flow direction can be induced by the variation of the flow channels and the entrance in the die section during the extrusion process [39]. The elongational deformation to which the material was subjected both during the filament extrusion process and FFF process appeared to be efficient in inducing a stable orientation of the filler platelets in the printing direction [40, 41].

Finally, tomographic analysis was employed to assess the distribution and volume of voids within the samples, as it allows observing sections of the samples at any chosen depth in all x, y, and z directions [42]. The presence of voids within components manufactured using FFF is inevitable, as they arise from the spaces between successive layers and within the paths of the deposited filament. Figure 6 presents scans of two mutually perpendicular sections of sample 3BN + 9T + 3BN. From these images, several porosities within the specimen can be observed. The voids are depicted in a color gradient indicating their volume; however, it is evident that these voids are limited in size,

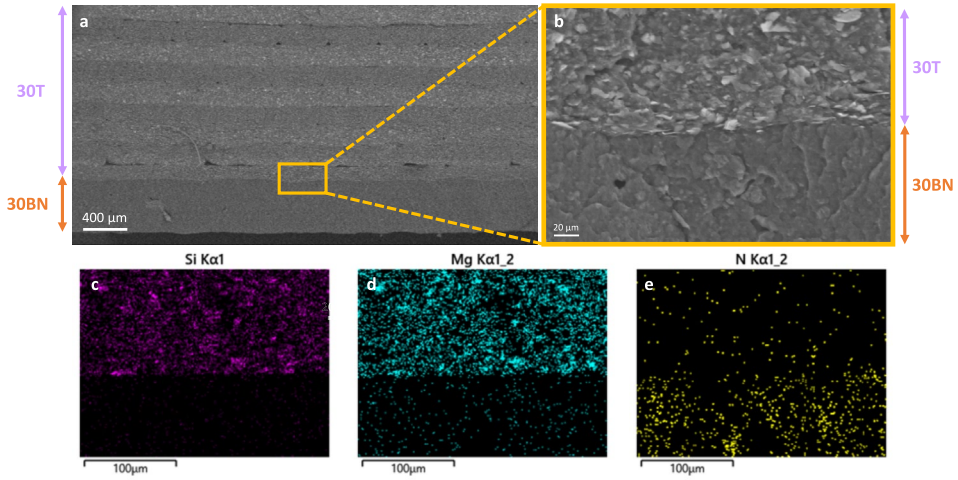

FIGURE 4 | (a) SEM image of the cross section of the sample 3BN + 9T + 3BN, (b) magnification 1000X of the interface between 30T and 30B layers and relative EDX mapping images of (c) Si, (d) Mg and (e) N.

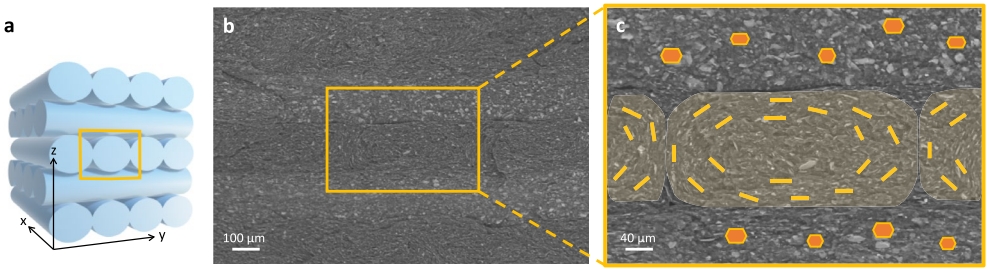

FIGURE 5 | (a) Schematic diagram of the filament orientation in the 3D printed samples, (b) SEM micrograph of the 30T layers in the 3BN + 12T sample, (c) enlargement of the cross-section with schematic illustration of the oriented filler.

ranging from 0.01 to 0.1 mm^3. Furthermore, they are distributed relatively uniformly throughout the entire height of the section, notwithstanding a preferential localization in the area closest to the lateral surface of the disk, resulting in a more compact center of the specimen with fewer defects. Nevertheless, it is interesting to observe that there is no preferential localization of voids at the interface between the surface layers containing boron nitride and those of the core containing talc, further demonstrating the excellent adhesion between the two composites, as previously indicated by the SEM analyses.

3.6 | Thermal Conductivity

To evaluate the effect of the amount of boron nitride on the final thermal conductivity of the specimen, initial measurements were conducted on PP, 15BN, 20BN, and 30BN. The results, reported in Figure 7a, revealed a consistent improvement in thermal conductivity with increasing the filler content both in the in-plane and through-plane directions. A similar improvement in thermal conductivity in PP/BN composites was observed by Chen et al. [43].

What is more interesting, however, is that the values of thermal conductivity in the radial direction of the specimen were consistently higher than those in the axial direction. This is primarily due to the FFF process itself, as the layer-by-layer deposition of the material means that 3D printed specimens are inherently characterized by defects and voids, especially in the axial direction. Indeed, considering the conductivity values at 0 wt% of BN, which should ideally be equal, the value in the in-plane direction is higher. Furthermore, an important contribution also comes from the preferential alignment of the filler in the printing direction, previously observed in the SEM micrographs (Figure 5), induced by the elongational flow to which the composite is subjected during extrusion, facilitating the formation of continuous conductive pathways in the IP direction compared to the TP direction.

Given these results, it was decided to localize the conductive material only in the surface layers, creating the skin-core structures previously described in Section 2.4. The comparison between the TP and IP conductivity values of the different structures is shown in Figure 7b. From these, it can be immediately observed that the 3D specimen 30BN shows conductivity values similar

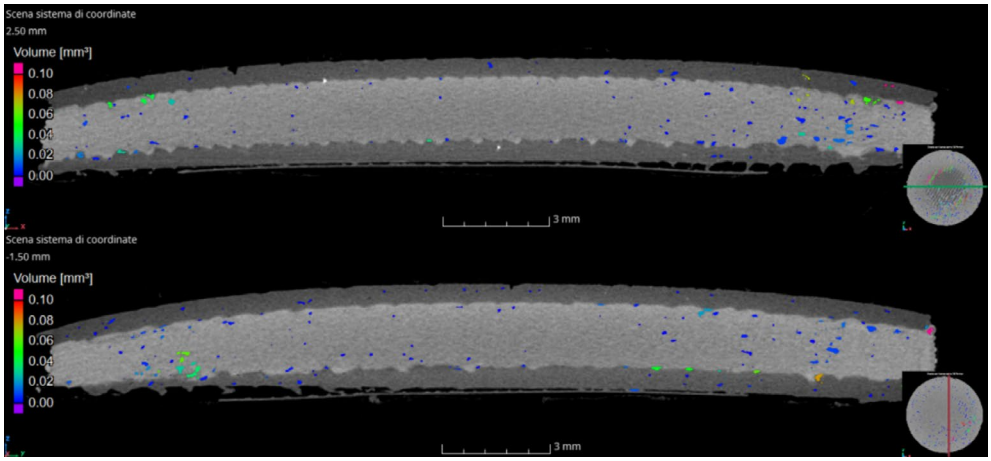

FIGURE 6 | X-ray computed tomography images of two sections of the 3BN + 9T + 3BN sample.

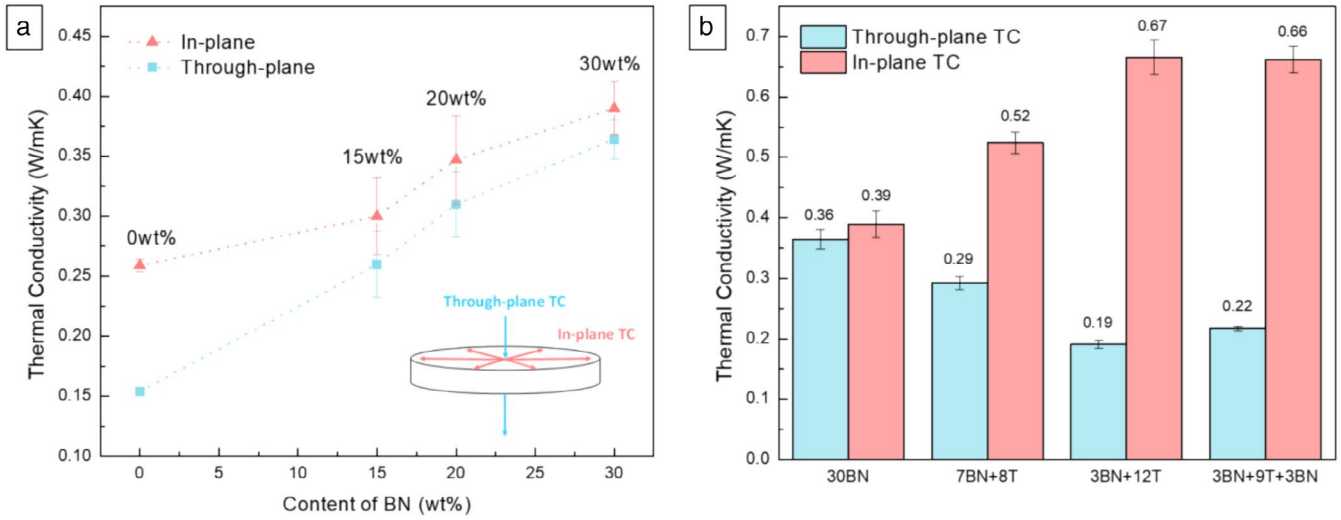

FIGURE 7 | (a) Thermal conductivity as a function of content of BN (the dotted lines are just an eye-guide), (b) comparison between the TC and IP thermal conductivity of the 3D printed samples.

in both directions. As the conductive layers containing BN are replaced by those reinforced with talc, decreasing from 15 in the 30BN sample to 7 in the 7BN + 8T specimen, and then to 3 in the 3BN + 12T and 3BN + 9T + 3BN specimens, there is a simultaneous increase in IP thermal conductivity and a decrease in TP thermal conductivity.

The decrease in TP conductivity is easily understood, as there is a gradual increase in the number of layers containing talc, which are less conductive, therefore hindering the transfer of thermal energy through the thickness of the specimen. However, the increase in IP thermal conductivity is less obvious and can be explained as follows. As mentioned in paragraph 3.4, talc-filled PP is more easily printable compared to BN-filled PP; therefore, the presence of some layers of 30T at the bottom of the sample allowed for the creation of a compact and well-adhered base on the printing platform, on which layers of 30BN could be deposited with better quality compared to the pure 30BN specimen, also owing to the excellent compatibility between the two composites. As a result, despite the reduction of the number of conductive layers from 15 to just 3, the IP TC value nearly doubled. These results indicate that to achieve a component capable of dissipating heat effectively, it is sufficient to localize the conductive filler in the uppermost layers of the sample. However, it is crucial to ensure good material deposition, as the presence of voids and defects can drastically worsen the conductivity properties. This allows for a reduction in the amount of conductive fillers required, resulting in cost savings. Additionally, if the second material is functionalized, it can lead to the creation of multifunctional components.

Considering the obtained thermal conductivity values, it can be observed that, despite the localization of the conductive filler solely in the surface layers, it was possible to achieve values of thermal conductivity similar to or even higher than those reported in the literature. For instance, Chen et al. [43], using a 20 wt% of BN, were only able to reach a maximum value of thermal conductivity of 0.45 W/mK. To achieve an even more significant increase in conductivity, it becomes essential to consider another important factor, that is the size of the BN lamellae. Indeed, some studies have demonstrated that, contrary to common belief, slightly thicker stacks of BN nanosheets with larger lateral size were better thermally conductive fillers [44]. Luo et al. [37], for example, explored the influence of filler size on thermal conductivity along different directions of 3D printed TPU specimens. Their study showed that larger size h-BN was more likely to orient to form better thermal conductive paths. In addition, the larger size filler had a smaller specific surface area and therefore lower interfacial thermal resistance between filler and matrix. In particular, with a 30 wt% of 27 μm h-BN, they were able to reach a value of thermal conductivity of 2.58 W/mK, which was 10 times that of pure TPU. Li et al. [35] also observed an increase in thermal conductivity with an increase in h-BN particle size from 4 to 27 μm, specifically from an in-plane TC value of 1.23 to 2.02 W/mK. In the case of this work, however, the BN platelets used were significantly smaller, measuring approximately 1 μm, making it much more challenging to achieve a continuous conductive pathway within the sample.

3.7 | Mechanical Properties

Regarding the mechanical properties, tensile tests were conducted on 30T and 30BN mono-material specimens as well as on skin-core structures 3BN + 12T and 3BN + 9T + 3BN. The values of elastic modulus and tensile stress are reported in Figure 8. It can be observed that the presence of boron nitride alone leads to the poorest mechanical performance, with average elastic modulus and maximum stress values of 600 and 13 MPa, respectively. A reduction in tensile strength, following the addition of BN, has also been observed by Chen et al. in their study on the effect of boron nitride on the mechanical properties of PP composites [43]. In contrast, as already extensively observed in many studies [45], talc has proven to be an excellent reinforcing filler, and a 30 wt% content resulted in the highest values of modulus and stress (average values of 1441 and 20 MPa, respectively). Concerning the skin-core structures, it is remarkable to observe that, despite the presence of layers containing BN and consequently one or two interfaces between the two different composites, they exhibit modulus and maximum stress values that are almost identical to those of the 30T specimens.

These results can be partly attributed to the fact that, in the combined specimens, the reinforced layers constitute the majority of the volume and the core of the sample, which largely determines its mechanical strength. Additionally, they are certainly a consequence of the excellent adhesion between the two composites, providing further evidence of their outstanding compatibility: the presence of talc-filled PP facilitated the deposition of higher-quality BN-filled layers, which consequently improved their mechanical performance.

The significance of these results becomes even more evident when compared to those reported in the literature. In fact, despite the presence of interfaces between the two composites, of BN-filled layers, and of the typical defects arising from the 3D printing process, the 3BN + 9T + 3BN specimen exhibits a tensile strength (20 MPa) equivalent to that reported by Wu et al. [46] for an injection-molded PP-based specimen containing 20 phr of talc.

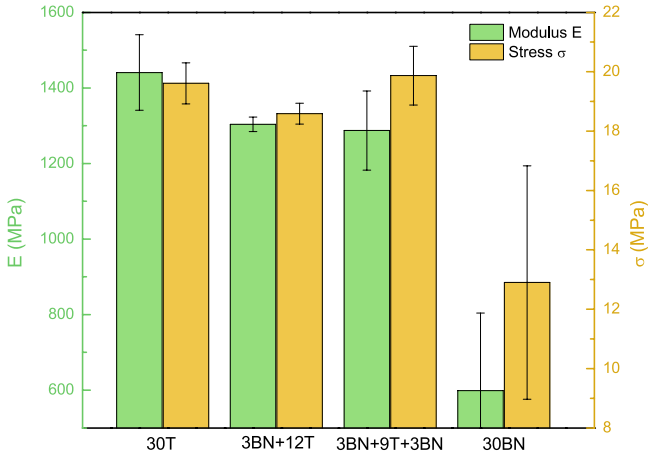

FIGURE 8 | Average values of elastic modulus and stress of tensile-tested 3D-printed specimens.

4 | Conclusions

This work has demonstrated the possibility of utilizing PP-based filaments functionalized with BN to 3D print objects with enhanced thermal conductivity, especially in the in-plane direction. Moreover, it has been demonstrated that by printing combined/skin-core structures in which only the topmost layers contain the conductive filler, while the layers within the core of the specimen contain a reinforcing filler, it is possible to simultaneously achieve good surface thermal conductivity and a significant enhancement of the mechanical properties. More specifically, as the number of conductive layers decreases and the number of talc-reinforced layers increases, the thermal conductivity in the through-plane direction is reduced, while that in the in-plane direction is increased. Simultaneously, from a mechanical perspective, these samples have demonstrated performance similar to the sample containing only talc, despite the presence of one or two interfaces between the two different composites. Therefore, the Fused Filament Fabrication process not only allows for the creation of a multi-material and multifunctional component in a single step but also results in an object that simultaneously exhibits improved in-plane thermal conductivity compared to the 30BN mono-material sample, while maintaining mechanical behavior comparable to that of the reinforced sample 30T. This work provides further evidence of the significant potential of 3D printing, particularly emphasizing the immense capabilities of polypropylene in this technique for creating innovative and highly customizable multi-material components.

Author Contributions

Conceptualization: R.A. and A.F. Methodology: E.L., R.A. and A.F. Formal analysis: E.L. Investigation: E.L. Writing – original draft preparation: E.L. Writing – review and editing: R.A. and A.F. Supervision: R.A. and A.F.

Acknowledgments

Open access publishing facilitated by Politecnico di Torino, as part of the Wiley - CRUI-CARE agreement.

Conflicts of Interest

The authors declare no conflicts of interest.

Data Availability Statement

The data that support the findings of this study are available from the corresponding author upon reasonable request.

References

1. E. Cuan-Urquizo, E. Barocio, V. Tejada-Ortigoza, R. B. Pipes, C. A. Rodriguez, and A. Roman-Flores, "Characterization of the Mechanical Properties of FFF Structures and Materials: A Review on the Experimental, Computational and Theoretical Approaches," *Materials* 12, no. 6 (2019): 895, https://doi.org/10.3390/ma12060895.

2. D. J. Roach, C. Roberts, J. Wong, et al., "Surface Modification of Fused Filament Fabrication (FFF) 3D Printed Substrates by Inkjet Printing Polyimide for Printed Electronics," *Additive Manufacturing* 36 (2020): 101544, https://doi.org/10.1016/j.addma.2020.101544.

3. X. Kuang, D. J. Roach, J. Wu, et al., "Advances in 4D Printing: Materials and Applications," *Advanced Functional Materials* 29, no. 2 (2019): 1805290, https://doi.org/10.1002/adfm.201805290.

4. M. J. Prajapati, A. Kumar, S. C. Lin, and J. Y. Jeng, "Multi-Material Additive Manufacturing With Lightweight Closed-Cell Foam-Filled Lattice Structures for Enhanced Mechanical and Functional Properties," *Additive Manufacturing* 54 (2022): 102766, https://doi.org/10.1016/j.addma.2022.102766.

5. S. W. Ahmed, G. Hussain, K. Altaf, et al., "On the Effects of Process Parameters and Optimization of Interlaminate Bond Strength in 3D Printed ABS/CF-PLA Composite," *Polymers* 12, no. 9 (2020): 2155, https://doi.org/10.3390/POLYM12092155.

6. D. Cao, D. Bouzolin, H. Lu, and D. T. Griffith, "Bending and Shear Improvements in 3D-Printed Core Sandwich Composites Through Modification of Resin Uptake in the Skin/Core Interphase Region," *Composites Part B: Engineering* 264 (2023): 110912, https://doi.org/10.1016/j.compositesb.2023.110912.

7. D. G. Bekas, Y. Hou, Y. Liu, and A. Panesar, "3D Printing to Enable Multifunctionality in Polymer-Based Composites: A Review," *Composites, Part B: Engineering* 179 (2019): 107540, https://doi.org/10.1016/j.compositesb.2019.107540.

8. M. Gomes, D. Martino, A. J. Pontes, and J. C. Viana, "Co-Injection Molding of Immiscible Polymers: Skin-Core Structure and Adhesion Studies," *Polymer Engineering and Science* 51, no. 12 (2011): 2398–2407, https://doi.org/10.1002/pen.22012.

9. R. Zhang, Z. Liu, Z. Sun, et al., "A Scalable Highly Thermal Conductive Silicone Rubber Composite With Orientated Graphite by Pre-Vulcanizing and Multilayer Stacking Method," *Composites. Part A, Applied Science and Manufacturing* 157 (2022): 106944, https://doi.org/10.1016/j.compositesa.2022.106944.

10. A. Regazzi, M. F. Pucci, L. Dumazert, et al., "Controlling the Distribution of Fire Retardants in Poly(Lactic Acid) by Fused Filament Fabrication in Order to Improve Its Fire Behaviour," *Polymer Degradation and Stability* 163 (2019): 143–150, https://doi.org/10.1016/j.polymdegradstab.2019.03.008.

11. A. Bandyopadhyay and B. Heer, "Additive Manufacturing of Multi-Material Structures," *Materials Science & Engineering R: Reports* 129 (2018): 1–16, https://doi.org/10.1016/j.mser.2018.04.001.

12. L. R. Lopes, A. F. Silva, and O. S. Carneiro, "Multi-Material 3D Printing: The Relevance of Materials Affinity on the Boundary Interface Performance," *Additive Manufacturing* 23 (2018): 45–52, https://doi.org/10.1016/j.addma.2018.06.027.

13. A. García-Collado, J. M. Blanco, M. K. Gupta, and R. Dorado-Vicente, "Advances in Polymers Based Multi-Material Additive-Manufacturing Techniques: State-Of-Art Review on Properties and Applications," *Additive Manufacturing* 50 (2022): 102577, https://doi.org/10.1016/j.addma.2021.102577.

14. M. Bertolino, D. Battegazzore, R. Arrigo, and A. Frache, "Designing 3D Printable Polypropylene: Material and Process Optimisation Through Rheology," *Additive Manufacturing* 40 (2021): 101944, https://doi.org/10.1016/j.addma.2021.101944.

15. Z. Zhang and X. Gao, "Polypropylene Random Copolymer Based Composite Used for Fused Filament Fabrication: Printability and Properties," *Polymers* 14, no. 6 (2022): 1106, https://doi.org/10.3390/polym14061106.

16. A. Das, N. Shanmugham, and M. J. Bortner, "Customized Blends of Polypropylene for Extrusion Based Additive Manufacturing," *Journal of Vinyl & Additive Technology* 29, no. 4 (2023): 649–661, https://doi.org/10.1002/vnl.21960.

17. R. T. L. Ferreira, I. C. Amatte, T. A. Dutra, and D. Bürger, "Experimental Characterization and Micrography of 3D Printed PLA and PLA Reinforced With Short Carbon Fibers," *Composites Part B: Engineering* 124 (2017): 88–100, https://doi.org/10.1016/j.compositesb.2017.05.013.

18. G. Bernagozzi, D. Battegazzore, R. Arrigo, and A. Frache, "Optimizing the Rheological and Thermal Behavior of Polypropylene-Based Composites for Material Extrusion Additive Manufacturing Processes," *Polymers* 15, no. 10 (2023): 2263, https://doi.org/10.3390/polym15102263.

19. T. Yamamoto, C. Luo, K. Ide, et al., "Fused Filament Fabrication and Mechanical Characterization of Hybrid Reinforced Polypropylene Composites With Talc Fillers and Cellulose Nanofibers," *Composites: Part A, Applied Science and Manufacturing* 188 (2025): 108536, https://doi.org/10.1016/j.compositesa.2024.108536.

20. S. Paszkiewicz, J. Andrzejewski, D. Grochała, et al., "Thinking Green on 3D Printing: Sustainable Polymer Compositions of Post-Consumer Polypropylene and Tire Rubber Crumbs Intended for Industrial Applications," *Materials* 17, no. 21 (2024): 5209, https://doi.org/10.3390/ma17215209.

21. C. G. Flores-Hernández, J. López-Barroso, C. E. Ramos-Galván, et al., "Development of a Composite Filament Based on Polypropylene and Garlic Husk Particles for 3D Printing Applications," *Applied Sciences* 14, no. 19 (2024): 9139, https://doi.org/10.3390/app14199139.

22. E. Lorenzi, R. Arrigo, and A. Frache, "Development of a Polypropylene-Based Material With Flame-Retardant Properties for 3D Printing," *Polymers* 16, no. 6 (2024): 858, https://doi.org/10.3390/polym16060858.

23. C. Aumnate, S. Limpanart, N. Soatthiyanon, and S. Khunton, "PP/Organoclay Nanocomposites for Fused Filament Fabrication (FFF) 3D Printing," *Express Polymer Letters* 13, no. 10 (2019): 898–909, https://doi.org/10.3144/expresspolymlett.2019.78.

24. L. An, Y. Yu, Q. Cai, S. Mateti, L. H. Li, and Y. I. Chen, "Hexagonal Boron Nitride Nanosheets: Preparation, Heat Transport Property and Application as Thermally Conductive Fillers," *Progress in Materials Science* 138 (2023): 101154, https://doi.org/10.1016/j.pmatsci.2023.101154.

25. L. Lapcik, P. Jindrova, B. Lapcikova, R. Tamblyn, R. Greenwood, and N. Rowson, "Effect of the Talc Filler Content on the Mechanical Properties of Polypropylene Composites," *Journal of Applied Polymer Science* 110, no. 5 (2008): 2742–2747, https://doi.org/10.1002/app.28797.

26. R. Arrigo and A. Frache, "FDM Printability of PLA Based-Materials: The Key Role of the Rheological Behavior," *Polymers* 14, no. 9 (2022): 1754, https://doi.org/10.3390/polym14091754.

27. H. Münstedt, "Rheological Measurements and Structural Analysis of Polymeric Materials," *Polymers* 13, no. 7 (2021): 1123, https://doi.org/10.3390/polym13071123.

28. T. Beran, T. Mulholland, F. Henning, N. Rudolph, and T. A. Osswald, "Nozzle Clogging Factors During Fused Filament Fabrication of Spherical Particle Filled Polymers," *Additive Manufacturing* 23 (2018): 206–214, https://doi.org/10.1016/j.addma.2018.08.009.

29. X. Zhang, L. Chen, C. Kowalski, T. Mulholland, and T. A. Osswald, "Nozzle Flow Behavior of Aluminum/Polycarbonate Composites in the Material Extrusion Printing Process," *Journal of Applied Polymer Science* 136, no. 12 (2019): 47252, https://doi.org/10.1002/app.47252.

30. J. R. Stockdale, S. A. Legett, X. M. Torres, et al., "Boron-Polymer Composites Engineered for Compression Molding, Foaming, and Additive Manufacturing," *Journal of Applied Polymer Science* 141, no. 16 (2024): 55236, https://doi.org/10.1002/app.55236.

31. X. Gao, S. Qi, X. Kuang, Y. Su, J. Li, and D. Wang, "Fused Filament Fabrication of Polymer Materials: A Review of Interlayer Bond," *Additive Manufacturing* 37 (2021): 101658, https://doi.org/10.1016/j.addma.2020.101658.

32. A. Kościuszko, D. Marciniak, and D. Sykutera, "Post-Processing Time Dependence of Shrinkage and Mechanical Properties of Injection-Molded Polypropylene," *Materials* 14, no. 1 (2020): 22, https://doi.org/10.3390/ma14010022.

33. D. Vaes, M. Coppens, B. Goderis, W. Zoetelief, and P. van Puyvelde, "Assessment of Crystallinity Development During Fused Filament Fabrication Through Fast Scanning Chip Calorimetry," *Applied Sciences* 9, no. 13 (2019): 2676, https://doi.org/10.3390/app9132676.

34. D. Vaes and P. van Puyvelde, "Semi-Crystalline Feedstock for Filament-Based 3D Printing of Polymers," *Progress in Polymer Science* 118 (2021): 101411, https://doi.org/10.1016/j.progpolymsci.2021.101411.

35. J. Li, J. Leng, Y. Jiang, and J. Zhang, "Experimental Characterization of 3D Printed PP/h-BN Thermally Conductive Composites With Highly Oriented h-BN and the Effects of Filler Size," *Composites. Part A, Applied Science and Manufacturing* 150 (2021): 106586, https://doi.org/10.1016/j.compositesa.2021.106586.

36. A. Sola, "Materials Requirements in Fused Filament Fabrication: A Framework for the Design of Next-Generation 3D Printable Thermoplastics and Composites," *Macromolecular Materials and Engineering* 307, no. 10 (2022): 2200197, https://doi.org/10.1002/mame.202200197.

37. M. Luo, T. Yang, T. Wang, Z. Yan, and J. Zhang, "The Effect of Filler Size on the Properties of TPU / BN Flexible Thermal Conductive Composites Prepared by Fused Filament Fabrication," *Polymer* 296 (2024): 126810, https://doi.org/10.1016/j.polymer.2024.126810.

38. Y. Jia, H. He, Y. Geng, B. Huang, and X. Peng, "High Through-Plane Thermal Conductivity of Polymer Based Product With Vertical Alignment of Graphite Flakes Achieved via 3D Printing," *Composites Science and Technology* 145 (2017): 55–61, https://doi.org/10.1016/j.compscitech.2017.03.035.

39. R. Arrigo, G. Malucelli, and F. P. Mantia, "Effect of the Elongational Flow on the Morphology and Properties of Polymer Systems: A Brief Review," *Polymers* 13, no. 20 (2021): 3529, https://doi.org/10.3390/polym13203529.

40. K. Markandan and C. Q. Lai, "Fabrication, Properties and Applications of Polymer Composites Additively Manufactured With Filler Alignment Control: A Review," *Composites, Part B: Engineering* 256 (2023): 110661, https://doi.org/10.1016/j.compositesb.2023.110661.

41. K. Niendorf and B. Raeymaekers, "Additive Manufacturing of Polymer Matrix Composite Materials With Aligned or Organized Filler Material: A Review," *Advanced Engineering Materials* 23, no. 4 (2021): 2001002, https://doi.org/10.1002/adem.202001002.

42. M. R. Khosravani and T. Reinicke, "On the Use of X-Ray Computed Tomography in Assessment of 3D-Printed Components," *Journal of Nondestructive Evaluation* 39, no. 4 (2020): 75, https://doi.org/10.1007/s10921-020-00721-1.

43. H. Chen, Y. Wang, Y. Nan, et al., "Effects of BN on the Mechanical and Thermal Properties of PP/BN Composites," *Journal of Wuhan University of Technology Materials Science Edition* 39, no. 2 (2024): 345–352, https://doi.org/10.1007/s11595-024-2890-x.

44. K. Sato and Y. Imai, "The Optimal Dimensions of Hexagonal-Boron Nitride Nanosheets as Thermally Conductive Fillers: The Thinner the Better?," *Current Opinion in Solid State & Materials Science* 29 (2024): 101143, https://doi.org/10.1016/j.cossms.2024.101143.

45. L. Altay, M. Sarikanat, M. Salam, T. Uysalman, and Y. Seki, "The Effect of Various Mineral Fillers on Thermal, Mechanical, and Rheological Properties of Polypropylene," *Research on Engineering Structures and Materials* 7, no. 3 (2021): 361–373, https://doi.org/10.17515/resm2021.258ma0213.

46. J. H. Wu, C. W. Chen, Y. T. Wu, G. T. Wu, M. C. Kuo, and Y. Tsai, "Mechanical Properties, Morphology, and Crystallization Behavior of Polypropylene/Elastomer/Talc Composites," *Polymer Composites* 36, no. 1 (2015): 69–77, https://doi.org/10.1002/pc.22914.

Supporting Information

Additional supporting information can be found online in the Supporting Information section.